

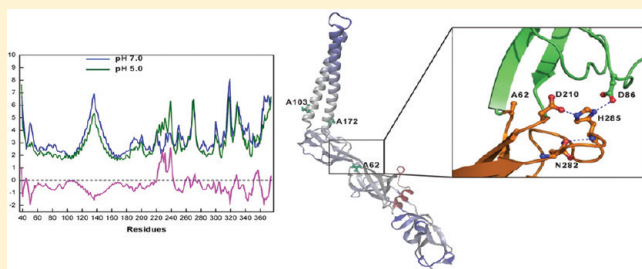
Interdomain Flexibility and pH-Induced Conformational Changes of AcrA Revealed by Molecular Dynamics Simulations

Beibei Wang[†], Jingwei Weng[‡], Kangnian Fan,[†] and Wenning Wang^{*,†,‡}

Shanghai Key Laboratory of Molecular Catalysis and Innovative Materials, [†]Department of Chemistry and [‡]Institutes of Biomedical Sciences, Fudan University, Shanghai, P.R. China

 Supporting Information

ABSTRACT: The membrane fusion protein (MFP) AcrA is proposed to link the inner membrane transporter AcrB and outer membrane protein TolC, forming the tripartite AcrAB–TolC efflux pump, and was shown to be functionally indispensable. Structural and EPR studies showed that AcrA has high conformational flexibility and exhibited pH-induced conformational change. In this study, we built the complete structure of AcrA through homology modeling and performed atomistic simulations of AcrA at different pH values. It was shown that the conformational flexibility of AcrA originates from the motions of α -hairpin and MP domains. The conformational dynamics of AcrA is sensitive to specific point mutations and pH values. In agreement with the EPR experiments, the interdomain motions were restrained upon lowering pH from 7.0 to 5.0 in the simulations. It was found that the protonation/deprotonation of His285 underlies the pH-regulated conformational dynamics of AcrA by disturbing the local hydrogen bond interactions, suggesting that the changes of pH in the periplasm accompanying the drug efflux could act as a signal to trigger the action of AcrA, which undergoes reversible conformational rearrangement.



1. INTRODUCTION

Gram-negative bacteria, such as *Escherichia coli*, have two layers of membranes, the inner and the outer membranes, separated by the periplasmic space. Multidrug efflux pumps,¹ which span the two layers of the membrane, can export a wide range of molecules out of the cell. The RND-type multidrug efflux pumps are largely responsible for intrinsic resistance in Gram-negative bacteria. AcrAB–TolC from *Escherichia coli* is one of the best characterized RND-type multidrug efflux systems composed of three essential components. The RND inner membrane protein AcrB assembles into a trimer with structural asymmetry, energized by the proton motive-force to pump the substrates across the inner membrane.^{2–7} The outer membrane protein (OMP) TolC is also trimeric and a cylindrical channel embedded in the outer membrane.^{8–10} Periplasmic protein AcrA is the third component of the multidrug efflux system that belongs to the membrane fusion protein (MFP) family. AcrA was shown to interact directly with both AcrB and TolC and is indispensable for the efflux function of the tripartite AcrAB–TolC pump system.^{11–15}

Crystal structures of AcrA and its homologues demonstrated that MFPs are elongated, sickle-shaped molecules consisting of four domains: a α -hairpin domain, a lipoyl domain, a β -barrel domain, and a membrane proximal (MP) domain¹⁶ (Figure 1A). In the crystal structure of AcrA, only three domains (α -hairpin, lipoyl, and β -barrel) were resolved.¹⁷ The MP domain, however, was shown to be functionally important¹⁵ and resolved in AcrA homologue MexA.¹⁸ Given the high sequence

similarity between AcrA and MexA (73%), it is reasonable to speculate that the N- and C-terminal region of AcrA also fold into a MP domain with similar structure with that in MexA. The α -helical hairpin domain of AcrA was shown to bind the outer membrane protein TolC, while the other domains interact with AcrB.^{13,14,19,20} In some MFPs, the β -barrel domain was found to be involved in ligand binding.^{21–24}

Crystal structures showed that AcrA, as well as its homologues, has large conformational flexibility. The conformational flexibility exhibited in the crystal structure of AcrA largely comes from the relative motions between the α -hairpin and lipoyl domains.¹⁷ Molecular dynamics simulations of the partial structure of MexA without MP domain revealed the similar conformational flexibility.²⁵ In the recently solved crystal structure of MexA, the MP domain adopts two distinct orientations with respect to the other part of the protein,¹⁸ suggesting high mobility of MP domain. Interestingly, the conformational flexibility and aggregation state of AcrA was reported to be reversely regulated by the pH condition.²⁶ The EPR studies showed that lowering the buffer pH from 7.0 to 5.0 caused the peaks of residues 62, 103, and 172 to become broadened, suggesting that these residues were in a more restricted environment.²⁶ Acidic pH also caused oligomerization of AcrA and affected the interaction between AcrA and

Received: December 19, 2011

Revised: February 6, 2012

Published: February 17, 2012



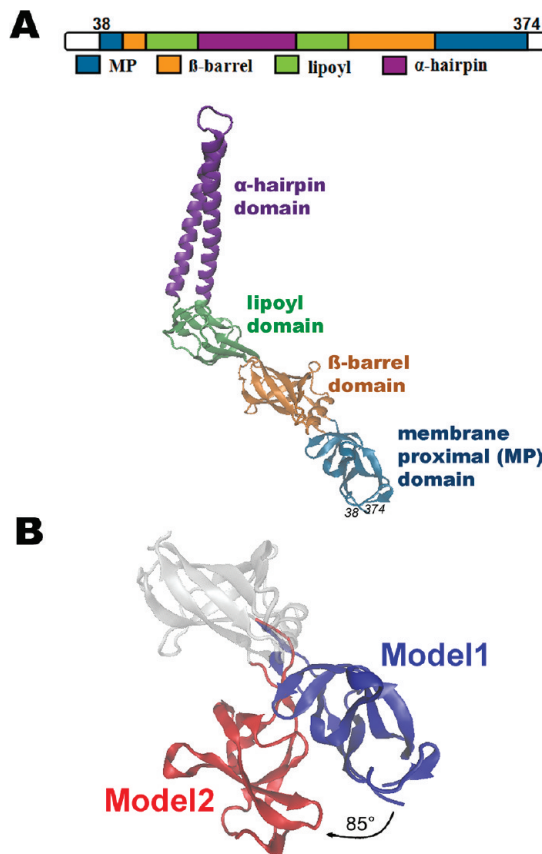


Figure 1. Domain organization and structures of AcrA. (A) The complete model structure of AcrA (38–374) built based on the crystal structure of MexA. (MP domain, blue; β -barrel domain, orange; lipoyl domain, lime; α -hairpin domain, purple.) (B) The two conformations of MP domain in Model 1 and Model 2.

AcrB.²⁶ Recent studies suggested that AcrA functions in a dimeric unit and assembles into a hexamer in the AcrAB–TolC complex.^{27,28} Furthermore, the conformational change of AcrA affects the assembly of the tripartite complex of AcrAB–TolC.²⁸ Taken together, cumulated experimental evidence showed that AcrA plays a key role in the efflux function of the tripartite pump AcrAB–TolC, and its function is sensitive to its conformational change and oligomeric state. However, the detailed molecular mechanisms of this function–structure and function–conformational dynamics relationships remain elusive. Atomistic details of the conformational dynamics of AcrA would be important for our understanding of the mechanism.

In this work, we provide the atomic details of the conformational dynamics of AcrA with MD simulations. Two complete structure models of AcrA with MP domain were built and one of them was found to be more stable in solution. The conformational flexibility of AcrA was shown to be dominated by the motion of MP and α -hairpin domains. His285 at the β -barrel domain was identified as a regulatory key of the pH-induced conformational change.

2. METHODS

2.1. Homology Modeling. The MP domain of AcrA was modeled by using Swiss model²⁹ based on the structure of MexA (PDBID: 2V4D; molecule F and H). There are two different conformations of MexA in the crystal structure with different MP domain orientations. Both conformations were

used as templates in model building, giving rise to two AcrA models (38–374). Then, the two models were fitted to the crystal structure of AcrA (53–299) taken from PDB database (PDBID: 2F1M; molecule C), with the $C\alpha$ rmsd less than 0.1 Å. The α -hairpin, lipoyl, and β -barrel domains in the two AcrA models were replaced by the corresponding domain structures in the AcrA crystal structure. Therefore, two models of AcrA with four domains (Model 1 and Model 2) were obtained.

2.2. Molecular Dynamics Simulation. All energy minimizations and MD simulations were carried out by using NAMD 2.6³⁰ and the CHARMM27³¹ force field. TIP3P model³² was used for water molecules. The pressure and temperature were maintained at 1 atm and 300 K by using the Nosé–Hoover piston method and Langevin dynamics with a damping coefficient of 1.0 ps^{−1}, respectively. The nonbonded interactions were truncated at a distance of 12 Å and smoothed by a switching function at 10 Å. The particle-mesh Ewald (PME) method was employed to compute electrostatic interactions.³³ All the bonds between hydrogen and the atom to which it is bonded were kept rigid using the SHAKE algorithm, and a time step of 2 fs was used. The whole system contains about 57 000 atoms including 249 water molecules. The whole system was first energy-minimized by 5000 steps. The solvent was then equilibrated for 2 ns with the protein constrained by harmonic forces, and then the whole system was subjected to a 20 ns long production run without any constraint. For each simulation system, three independent trajectories with different initial velocities were conducted. The root-mean-square fluctuation (rmsf) of $C\alpha$ and the distributions of α and θ were calculated using the structural ensembles of all three trajectories. The data analyses were performed by using VMD.³⁴

pK_a values of titratable residues in AcrA were calculated using H⁺⁺,³⁵ and the protonation states of residues were determined according to the calculated pK_a values. The protonated residues in Model 1 at pH 5.0 are Asp144, 149, 222, 320, 330, Glu229, 261, 298, and His285. For Model 2, one more residue was protonated (Glu333) at pH 5.0.

2.3. Cluster Analysis. The rmsd-based GROMOS algorithm³⁶ was used for the cluster analysis of the MD trajectories. The conformations of AcrA were extracted from all three trajectories for each system at 0.005 ns intervals. For each pair of structures, a least-squares translational and rotational fit of the lipoyl domain was performed. In the clustering process, the difference between two structures was evaluated by the rmsd of the backbone atoms, and the cutoff value was set to 5 Å.

3. RESULTS

3.1. Molecular Modeling of the Complete Structure of AcrA (38–374). Previous study solved the crystal structure of an AcrA fragment containing the α -hairpin, lipoyl, and β -barrel domains with four residues mutated (F223M, L224M, L287M, and L288M).¹⁷ This partial structure does not contain the membrane-proximal (MP) domain, which was shown to be important for the function of the AcrAB–TolC complex.¹⁵ To obtain the complete the structure of AcrA, we built the MP domain of AcrA through molecular modeling using the structure of MexA as template¹⁸ (see Methods for more detail). In the crystal structure of MexA, the MP domain exhibits two distinct orientations with respect to the other domains in the protein.¹⁸ Therefore, two models (Model 1 and

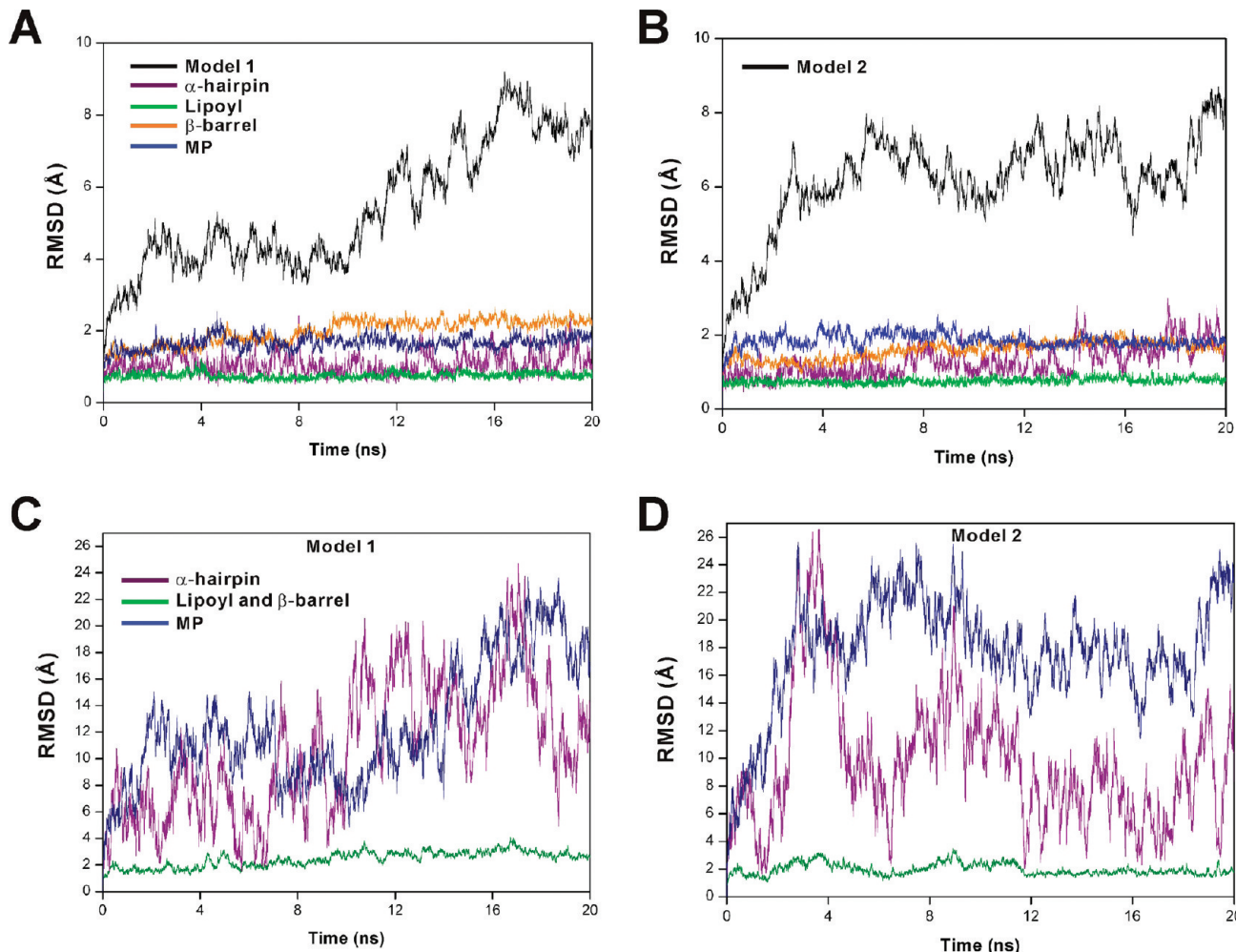


Figure 2. C_α rmsds along the MD simulation trajectories of wild-type AcrA. The C_α rmsds of the whole protein and the individual domains for Model 1 (A) and Model 2 (B). The rmsds of MP, α -hairpin, lipoyl, and β -barrel domains in Model 1 (C) and Model 2 (D) calculated by fitting the frames onto the lipoyl and β -barrel domains.

Model 2) of AcrA (38–374) were built with different MP domain orientations similar with those in MexA¹⁸ (Figure 1B).

3.2. Conformational Dynamics of Wild-Type AcrA (38–374). For the simulations of wild-type AcrA, the four methionine substitutions in the crystal structure of AcrA were mutated back to their wild-type residues. Both models of AcrA exhibited high conformational flexibility. The maximum root-mean-square deviation (rmsd) of C_α atoms with respect to the initial structure along the trajectories reached about 9 Å (Figure 2A,B). However, the rmsds of the four individual domains are much lower (~2 Å), indicating that the structures of individual domains are very stable (Figure 2A,B). Therefore, the conformational flexibility can be mainly attributed to interdomain motions. It is worth noting that the structure of MP domain built through molecular modeling is as stable as the other domains (Figure 2A,B). Among the four domains, the lipoyl domain exhibits extraordinary stability, with rmsds fluctuating around 1 Å (Figure 2A,B). By superimposing the frames of the trajectories on to the lipoyl and β -barrel domains, the calculated rmsds of α -hairpin or MP domains were very large (maximum values of ~24 Å for Model 1 and ~26 Å for Model 2), while that of the lipoyl and β -barrel domains remained small (Figure 2C,D). This demonstrates that the interdomain motions of AcrA are dominated by the movements

of α -hairpin and MP domains with respect to the lipoyl and β -barrel domains, which form a relatively rigid module. Experimentally, the crystal structures of AcrA demonstrated the conformational flexibility of the α -hairpin domain, the orientation of which in the four molecules in the asymmetric unit varies in a range of ~15°.¹⁷ Accordingly, analysis of the structure ensemble of our MD trajectories showed that the orientation of the α -hairpin domain also distributes in a range of ~15° with respect to the initial conformation (Figure 3A). Therefore, the conformational variation observed in the partial crystal structure of AcrA reflects the intrinsic conformational flexibility of the α -hairpin domain.

The conformational movement of the MP domain can be partly described by the variation of an angle (α) connecting the center of masses (COMs) of the lipoyl domain (L), the β -barrel domain (B), and the MP domain (M) (Figure 3B). In the initial structures, the values of angle α in Model 1 and Model 2 are around 160° and 132°, respectively. In the structure ensemble of the MD simulations, angle α has a broader distribution in Model 2 than in Model 1 (Figure 3C). The most probable values of α in Model 1 are close to the initial value, within a range of 10° (160–170°), while the distribution of α in Model 2 deviates from the initial value, with the highly probable values within the range of 135–155° (Figure 3C).

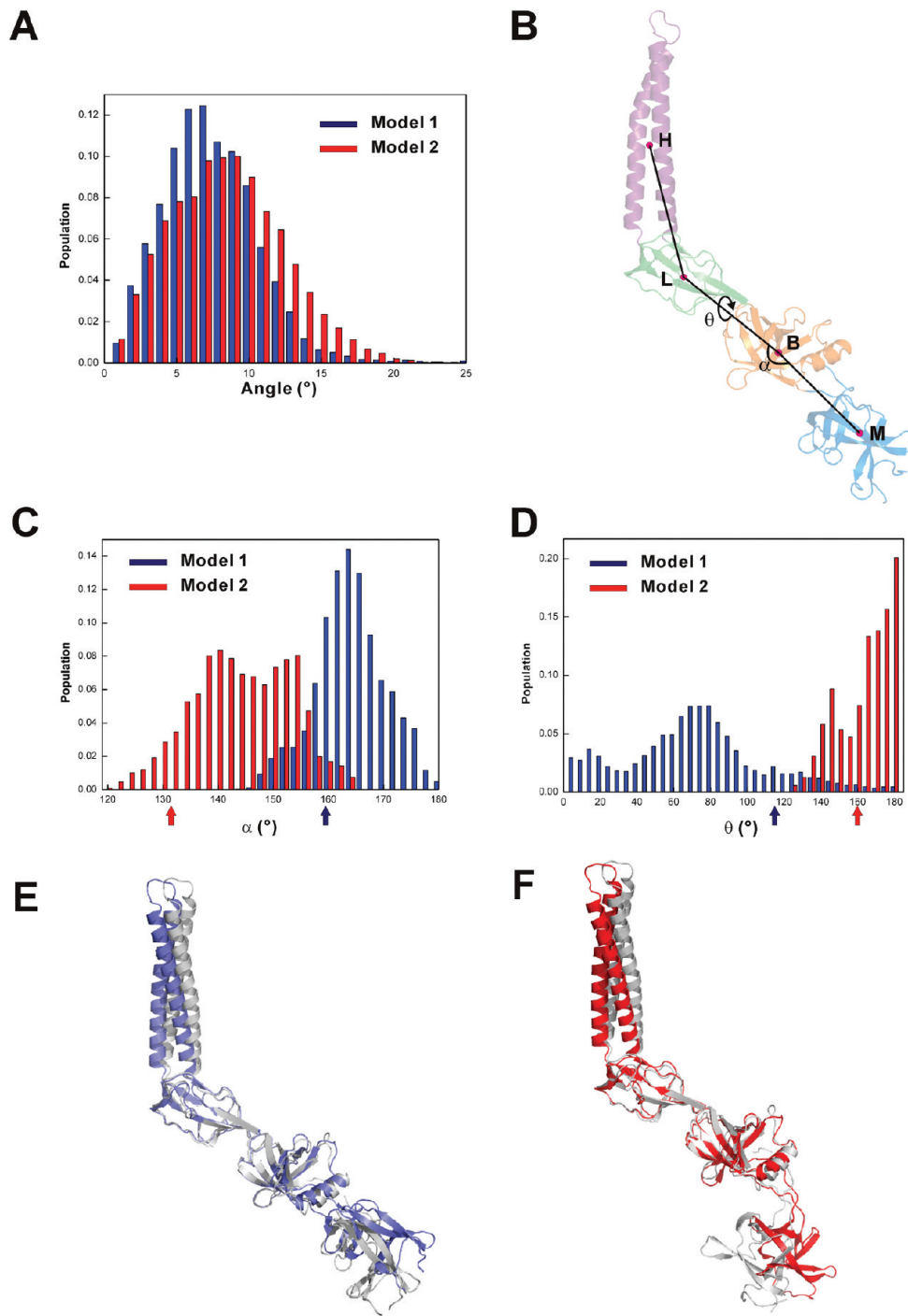


Figure 3. Conformational flexibility of wild-type AcrA. (A) The distributions of the bending angles of the α -helical domain with respect to the initial structure in Model 1 and Model 2. (B) α is defined by the center of masses (COMs) of the lipoyl domain (L), the β -barrel domain (B), and the MP domain (M). θ is defined as the dihedral angle connecting the COMs of the four domains (H, L, B, and M). (C) The population of α in the structure ensembles of the MD simulations for Model 1 (blue) and Model 2 (red). (D) The population of dihedral angle θ in the structure ensembles of the MD simulations for Model 1 (blue) and Model 2 (red). The arrows in panels C and D indicate the initial values of α or θ . (E) Comparison of the average structure of the largest cluster of Model 1 (blue) with its initial structure (white). (F) Comparison of the average structure of the largest cluster of Model 2 (red) with its initial structure (white).

Furthermore, a dihedral angle θ defined as connecting the COMs of the four domains was used to describe the interdomain motions (Figure 3B). The values of θ in Model 1 and Model 2 among the structure ensemble of MD trajectories span very different ranges, and the distribution of θ in Model 1 is much broader than that in Model 2 (Figure 3D), suggesting that Model 1 and Model 2 sample different

regions of conformational space. Cluster analysis of the conformation ensemble of the simulation trajectories showed that the populations of the first two clusters of Model 1 (39%, 18%) are slightly larger than those of Model 2 (23%, 11%). Comparison of the average structures of the largest cluster of Model 1 and Model 2 with their initial structures clearly

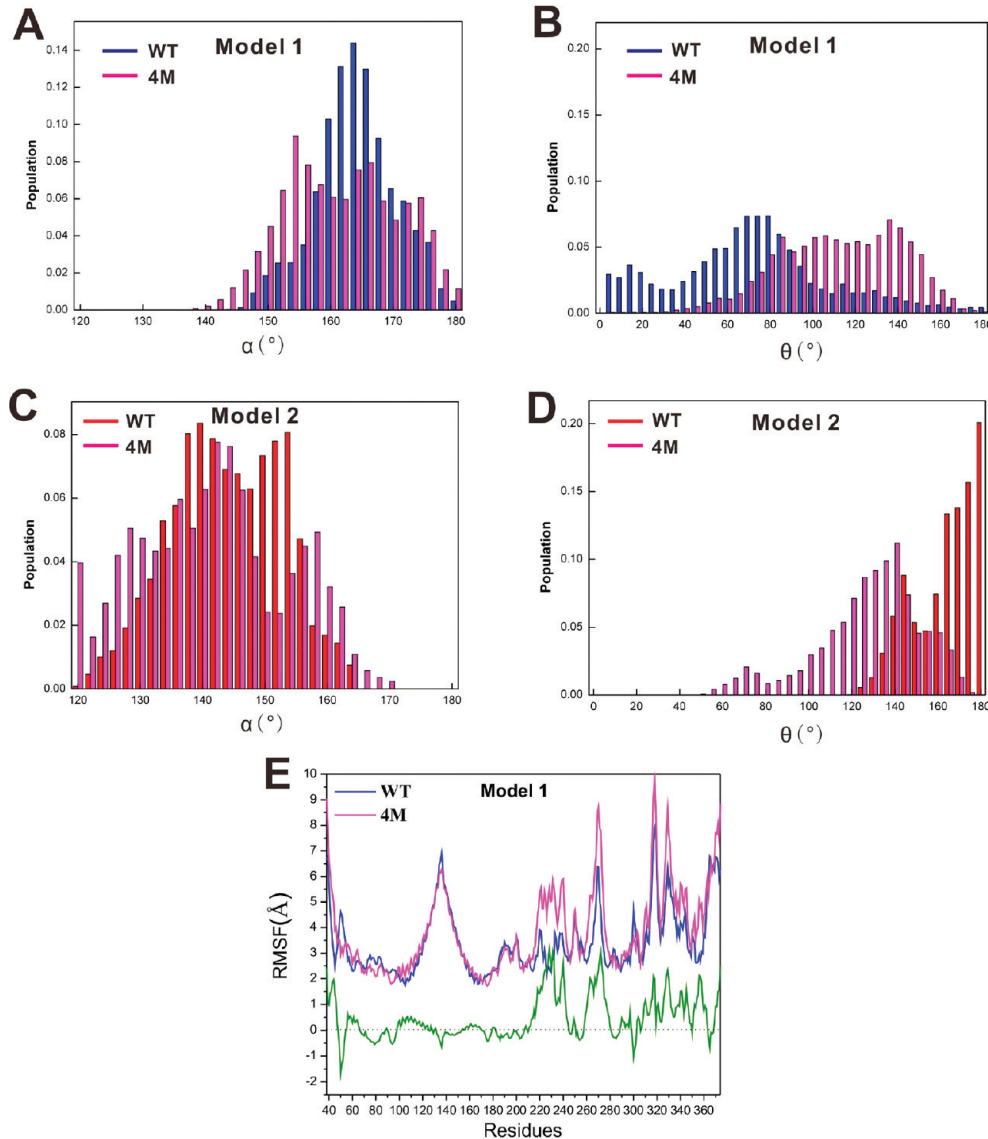


Figure 4. Conformational populations of AcrA-4M. The population of angle α (A,C) and dihedral angle θ (B,C) in the structure ensembles of MD simulations for Model 1-4M (A,B) and Model 2-4M (C,D), respectively, in comparison with the wild-type AcrA. (E) Comparison of the rmsfs of Ca atoms of wild-type Model 1 (blue) and Model 1-4M (magenta), with the rmsf difference shown in olivine. The rmsf differences are mapped on the ribbon diagram of the AcrA structure. Blue color denotes the reduced values of rmsf, and the red color denotes the increased ones.

showed the conformational changes at the α -hairpin domain and MP domain (Figure 3E,F).

Overall, simulation results demonstrated that AcrA (38-374) has remarkable conformational flexibility, mainly arising from the motions of the α -hairpin and MP domains relative to the other two domains.

3.3. Mutations in of AcrA (38-374)-4M Changed the Conformational Distributions. Previous experimental studies showed that the quadruple methionine substitution mutant AcrA-4M did not confer resistance to many kinds of drugs.¹⁷ High structural similarity between AcrA (45-312)-4M¹⁷ and its homologue MexA^{37,18} suggests that the mutations do not significantly change the protein structure. To examine the effect of the 4M mutations on the conformational dynamics of AcrA, we performed MD simulations on the AcrA (38-374)-4M mutant, the initial structures of which were the same as those of wild-type Model 1 and Model 2. Similar with the wild-type protein, two models of AcrA-4M exhibit conformational flexibility arising from the movements of α -hairpin and MP

domains with respect to the rest part of AcrA (Figure S1, Supporting Information). Structures of individual domains are stable, and the lipoyl and β -barrel domains form a rigid module as in the wild-type AcrA (Figure S1, Supporting Information).

Cluster analysis showed that the size of the largest cluster of Model 1-M is much smaller than that of Model 1-WT. The average structure of the largest cluster of Model 1-4M differs obviously from that of Model 1-WT, with the MP domain rotating an angle with respect to the wild-type protein (Figure S2, Supporting Information). Model 1-4M exhibits a more distinct θ distribution than that of Model 1-WT, while the distributions of α angles in WT and the mutant are very similar (Figure 4A,B). A similar situation was found in Model 2, in which the mutations changed the distribution of dihedral angle θ but not that of the angle α (Figure 4C,D). In both models, the value of θ increased, resulting in the elongation of the whole molecule, i.e., the protein adopted a more extended conformation upon mutation.

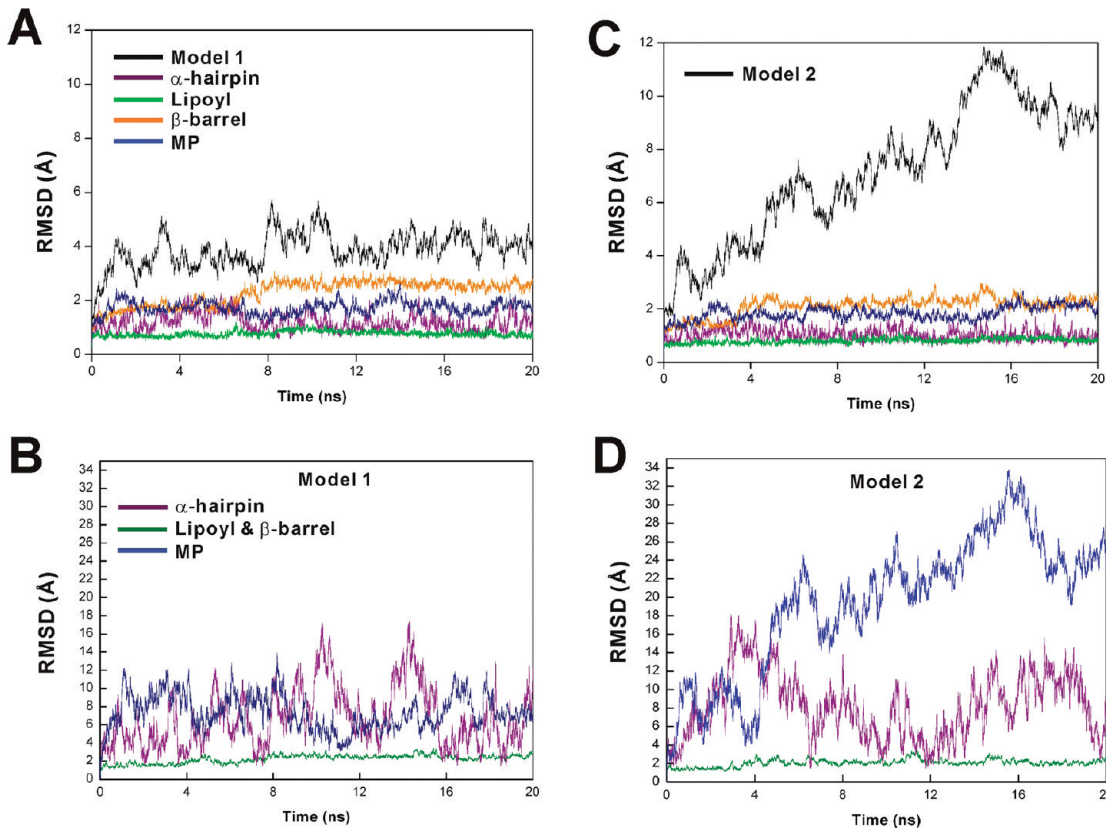


Figure 5. $\text{C}\alpha$ rmsds along the MD simulation trajectories of AcrA at pH 5.0. The $\text{C}\alpha$ rmsds of the whole protein and the individual domains for Model 1 (A) and Model 2 (B). The rmsds of MP, α -hairpin, lipoyl, and β -barrel domains in Model 1 (C) and Model 2 (D) calculated by fitting the frames onto the lipoyl and β -barrel domains.

The four methionine substitutions are all located in the β -barrel domain, two of them on the $\alpha 3$ helix (F223, L224) and the other two at the loop between $\beta 13$ and $\beta 14$ (L287, L288). Although these mutations did not disturb the domain structures as mentioned above, they perturbed the local backbone mobility of the β -barrel domain. The root-mean-square fluctuations (rmsf) of $\text{C}\alpha$ atoms during the MD simulations around the methionine substitution sites increased remarkably in Model 1-4M with respect to Model 1-WT (Figure 4E). Besides the β -barrel domain, the MP domain also exhibited larger rmsf upon mutations in Model 1, which may affect the interdomain motions.

3.4. Conformational Flexibility of AcrA Was Reduced upon Lowering pH. Previous EPR study of AcrA showed that the protein undergoes conformational changes upon lowering the buffer pH from 7.0 to 5.0.²⁶ Here, we calculated the pK_a of the titrated residues of AcrA at pH 5.0 (see Methods for more details) and performed MD simulations with the two models as initial structures at pH 5.0. Although the simulation results showed that AcrA still has remarkable conformational flexibility due to the interdomain motions at pH 5.0 (Figure 5), the acidification caused different behavior of AcrA compared with the system at pH 7.0. For Model 1, the conformational motions of AcrA were largely restricted. The $\text{C}\alpha$ rmsd relative to the initial structure along the trajectories fluctuated around 4.0 Å at pH 5.0, obviously smaller than the rmsd values at pH 7.0 (Figure 5A). By fitting the simulation frames on the lipoyl and β -barrel domains, the rmsds of α -hairpin or MP domains with respect to the initial structures were calculated. Compared with the system at pH 7.0, the rmsds were obviously smaller during

the last 10 ns (Figure 5B), indicating that the relative motions of both α -hairpin and MP domains are suppressed at pH 5.0. For Model 2, however, the simulation results showed that the $\text{C}\alpha$ rmsds did show obvious difference from that at pH 7.0 (Figure 5C). The MP domain of Model 2 underwent especially large scale conformational movement relative to lipoyl and β -barrel domains (Figure 5D). Comparison of the rmsfs at different pH conditions showed that the rmsf values of Model 1 decreased upon lowering pH in most of the regions of AcrA, except $\alpha 3$ and the loop between $\alpha 3$ and $\beta 11$ (Figure 6A). In agreement with the EPR experiment, the regions in the vicinities of residues Ala62, Ala103, and Ala172, which became more immobilized upon acidification, have decreased rmsfs in the simulations (Figure 6A). In contrast with Model 1, the rmsfs of Model 2 at pH 5.0 increased slightly in most regions of the protein (Figure S3, Supporting Information). It is worth noting, however, that the pattern of the rmsf difference is not totally consistent with the EPR experiments. For example, the residues with most prominent decreases of rmsfs locate at the tip of the α -hairpin domain and the MP domain, while no residues in these regions became more immobilized at pH 5.0 in the experiments. One reason for the discrepancies could be due to the intermolecular interactions at lower pH condition. At pH 5.0, spin-labeled Ala146, which locates at the tip of the α -hairpin, showed a very different EPR spectrum than that at the neutral condition, characterizing the involvement of intermolecular interactions. The conformational changes may interfere with the intermolecular interactions, which were not considered in our calculations. However, the EPR spectra mainly probe the mobility of the side chain of a spin-labeled

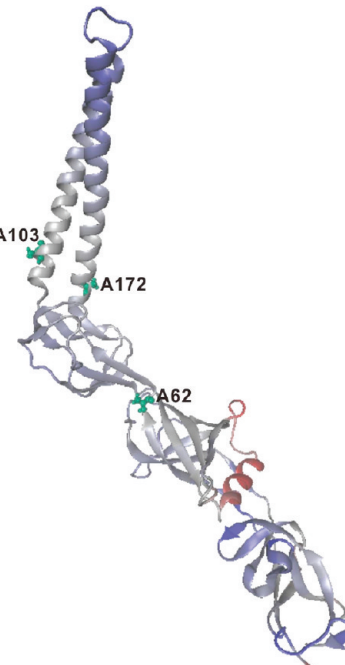
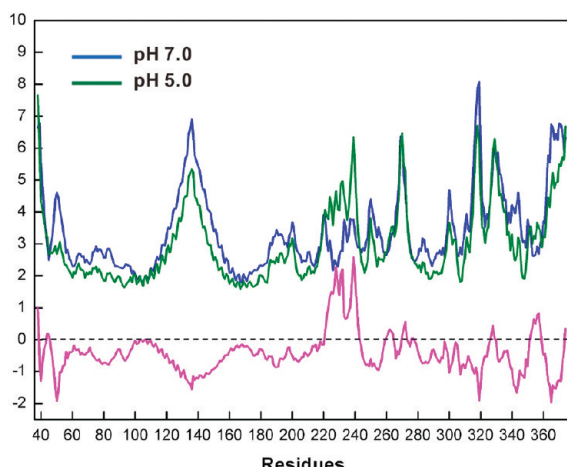
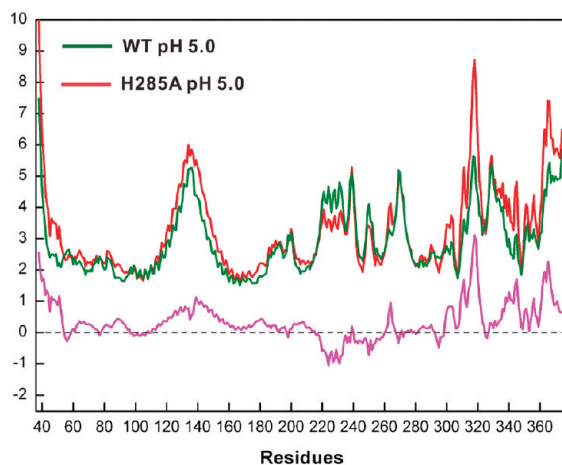
A**B**

Figure 6. pH conditions affect the rmsfs of AcrA. (A) Comparison of the rmsfs of Model 1 at pH 7.0 (blue) and pH 5.0 (green). The rmsf differences are shown in pink. (B) Comparison of the rmsfs of Model 1-WT (green) and H285A (red) at pH 5.0, with the rmsf differences shown in pink. The rmsf differences are mapped on the ribbon diagram of the AcrA structure as in Figure 4.

residue with a bulky spin label group, while the rmsfs of $\text{C}\alpha$ atoms reflect the backbone flexibility.

The distributions of α and θ at pH 5.0 are also different from those at pH 7.0. For Model 1, the distribution of α was similar with that at pH 7.0, but the distribution of the dihedral angles θ is narrower than that of pH 7.0, and the most probable values of θ is around the value of the initial conformation (Figure 7A,B). Consistent with this, the cluster analysis of the trajectories under pH 5.0 showed that the average structure of the largest cluster of Model 1 is very similar to the initial conformation (Figure 7E). For Model 2, the distribution of θ did not change much, while the α angle deviated largely from the initial value and exhibited different distribution from that at pH 7.0 (Figure 7C,D). The MP domain in the average structure of the largest cluster of Model 2 adopts a very

different orientation than that in the initial structure (Figure 7F).

3.5. Protonation State of His285 Regulates the pH-Induced Conformational Flexibility of AcrA. The reduced conformational flexibility of AcrA upon acidification in the simulations supports the experimental observations that at pH 5.0 several residues became more immobilized.²⁶ By careful examination of the intramolecular interactions in Model 1, we identified that the hydrogen bond interactions around His285 changed significantly upon acidification. At pH 7.0, His285 forms a side chain hydrogen bond with Asp210 and a backbone hydrogen bond with Asn282. His285 was protonated under pH 5.0, resulting in the formation of an additional strong hydrogen bond between His285 and Asp86 at the lipoyl domain (Figure 8A). At the same time, the other two hydrogen bonds around

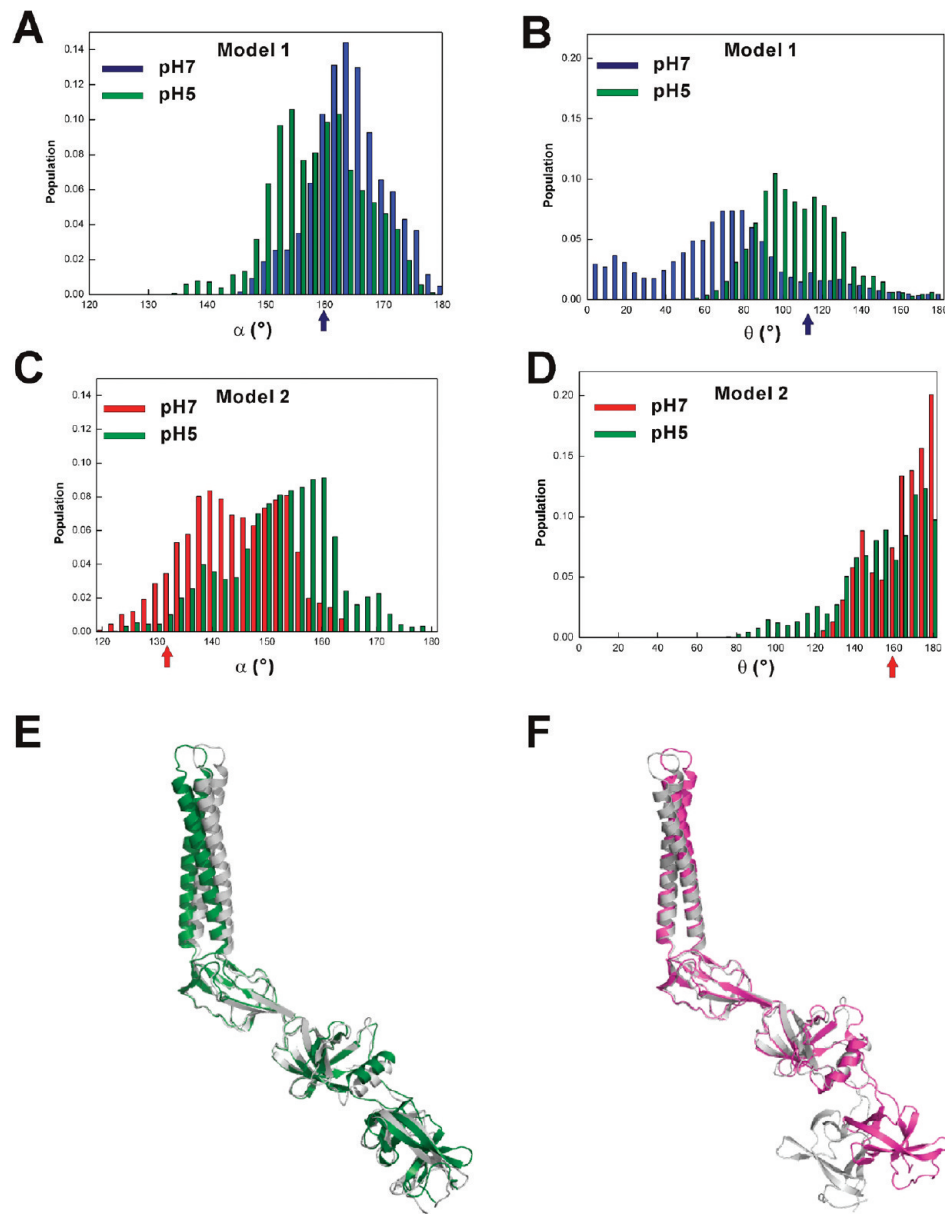


Figure 7. Conformational populations of AcrA at pH 5.0. The population of angle α (A,C) and dihedral angle θ (B,D) in the structure ensembles of MD simulations for Model 1 (A,B) and Model 2 (C,D) at pH 5.0, in comparison with the case at pH 7.0. The arrows indicate the initial values of α or θ . (E) Comparison of the average structure of the largest cluster of Model 1 at pH 5.0 (blue) with its initial structure (white). (F) Comparison of the average structure of the largest cluster of Model 2 at pH 5.0 (red) with its initial structure (white).

His285 were also strengthened at acidic pH (Figure 8B). This strong hydrogen bond network located at the linker region between lipoyl and β -barrel domain will obviously reduce the relative motions between these two domains. The rigidification may further reduce the conformational movement of α -hairpin and MP domains. In the EPR experiments, residue Ala62 displayed especially clear evidence of restricted motion at pH 5.0.²⁶ This residue locates in the vicinity of the hydrogen network around His285, which can stabilize the local structure at this region (Figure 8A).

In Model 2, however, the hydrogen bond between the protonated His285 and Asp86 was very weak, and the other two hydrogen bonds involving His285 were weakened at pH 5.0 (Figure 8B). The weakening of the hydrogen bond interactions may be caused by the large scale movement of MP domain in Model 2. Therefore, the dynamic behavior of

Model 2 did not agree with the experimental observation, suggesting that Model 2 might not be the most probable conformation of AcrA in solution.

To verify the role of His285 in the pH induced conformational change, we performed the MD simulations of the H285A mutant at pH 5.0. The calculated $C\alpha$ rmsfs showed that the H285A mutation obviously increases the conformational flexibility of AcrA at pH 5.0 (Figure 6B). The rmsf difference between the wild-type and H285A mutant demonstrated that the MP domain and α -hairpin domain became more flexible upon mutation. These results confirmed that His285 plays a role in the pH-induced conformational change of AcrA.

4. DISCUSSION

Our understanding of the working mechanism of the tripartite drug efflux system AcrAB–TolC has been boosted during the

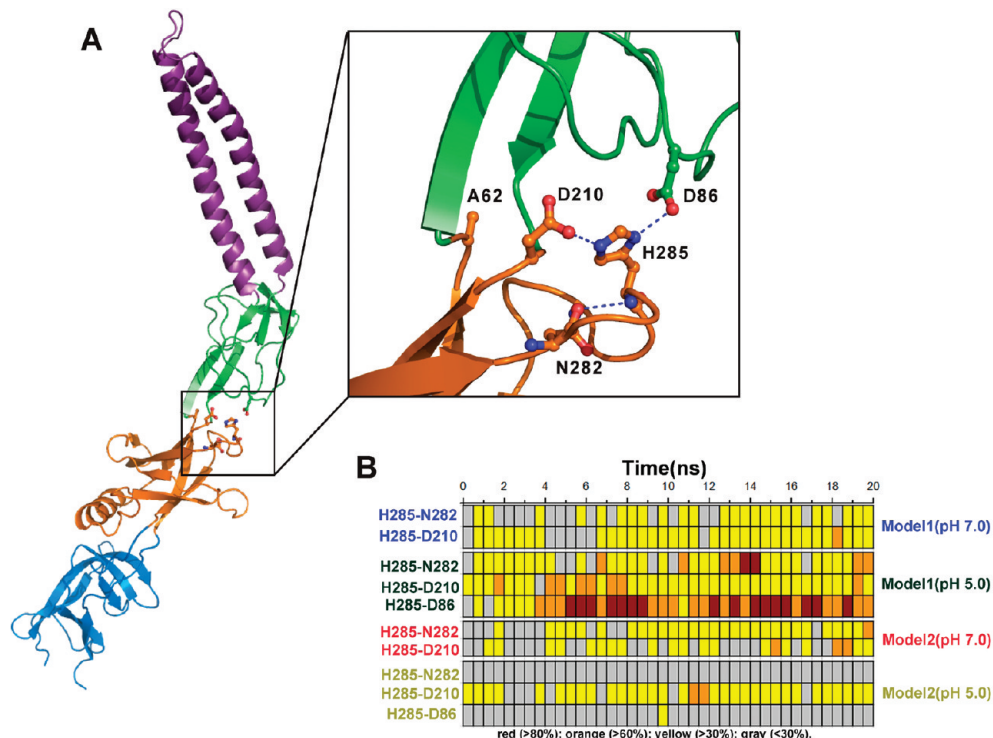


Figure 8. Hydrogen bond network around His285 is affected by the pH conditions. (A) The hydrogen bond interactions around His285 at pH 5.0 in Model 1. (B) Variation of the hydrogen bond interactions around His285 throughout the simulation time. Each grid represents 0.5 ns, and its color corresponds to the percentage of hydrogen bond emergence in this period (red, >80%; orange, >60%; yellow, >30%; and gray, <30%). The hydrogen bond cutoffs are set by the donor–acceptor distance being less than 3.5 Å and the deviation of the donor–hydrogen–acceptor angle less than 30° from 180°.

past decade, mainly due to the crystal structures of each individual part of the complex.^{18,27} Among them, the membrane fusion protein (MFP), AcrA, has been shown to be indispensable for function and was proposed to link AcrB and TolC into a tripartite assembly. The crystal structures of AcrA and its close homologous demonstrated that it has an elongated sickle shape with conformational diversity, which may have potential functional significance in the tripartite complex. Here, we built the complete model structure of AcrA, based on the partial structure of AcrA and the intact structure of MexA, and explored its conformational dynamics with atomistic simulation.

Consistent with the structural studies, MD simulations showed that both α -hairpin and MP domains underwent significant conformational movement, whereas the lipoyl and β -barrel domains form a relatively rigid module. The initial structure of the simulation resembles the conformation of Molecule C in the AcrA (45-312) crystal. The resultant bending angle distribution covered the range of conformational diversity in the crystal and demonstrated that the most probable bending angles are close to those in Molecules A and D. In the crystal structure of MexA, however, the α -hairpin domain did not exhibit conformational flexibility, with the bending angle close to Molecule D in AcrA crystal.^{18,37} This is most likely due to the intermolecular packing in the MexA crystal, in which thirteen molecules in an asymmetric unit pack to form a cylinder through their α -hairpin domains. Moreover, previous MD simulations of MexA without MP domain also revealed the conformational movement of α -hairpin domain in monomeric state.²⁵ Therefore, the hinge bending motion of the α -hairpin domain reflects the intrinsic conformational flexibility

of monomeric AcrA (MexA), and the MD simulation trajectories likely have sampled the complete hinge bending conformational space of the α -hairpin domain.

Both proteolytic digestion experiments and structural studies demonstrated that the MP domain is highly flexible.^{17,37} In MD simulations, we started from two distinct conformations of MP domain based on the MexA structures.¹⁸ The results showed that MP domain samples large conformational spaces in both Model 1 and Model 2. The conformational spaces of two models have little overlap. This may be due to the incomplete sampling in the MD simulation. However, as we will discuss below, Model 1 likely represents the more stable state of monomeric AcrA in solution. However, the conformational movement of MP domain was turned out to be sensitive to local modifications, such as the 4M substitution. Without disturbing the domain structures, the 4M mutation obviously changed the conformational distribution of AcrA. Although further tests are required to identify the exact cause of the loss of function in AcrA-4M, the change of conformational dynamics provides clues for understanding this phenomenon.

The most interesting finding in this study is that lowering pH to 5.0 reduced the conformational flexibility of AcrA, which is in agreement with the previous EPR experiments.²⁶ In addition, acidification was shown to stabilize the conformation of Model 1, while the conformational flexibility of Model 2 was insensitive to pH values. In this respect, Model 1 is most likely the stable state of AcrA in solution, while the conformation of MP domain in Model 2 may result from the crystal packing. The pH regulated conformational change may have potential functional role in the tripartite AcrAB–TolC assembly. In *E. coli*, about half of the proton motive force across

the cytoplasmic membrane comes from a proton gradient, with the cytoplasmic pH being higher than the external pH by about 1.7 pH units.³⁸ Therefore, coupling with the transport of substrates, the pH value of the periplasm varies significantly. Recent studies provide evidence that the functional oligomeric state of AcrA is trimer or dimer,^{27,28} and acidic pH promotes the oligomerization of AcrA.^{26,28} Therefore, the pH-induced conformational flexibility changes may underlie the regulation of the oligomeric state of AcrA. The reduced conformational flexibility can favor the intermolecular packing and reduce the entropy cost of oligomerization. However, it was shown that lowering pH significantly enhances the binding affinity between AcrA and AcrB.²⁸ Therefore, the changes of pH in the periplasm accompanying the drug efflux could also act as a signal to regulate the assembly of the tripartite AcrAB–TolC complex.

■ ASSOCIATED CONTENT

S Supporting Information

A figure of the $C\alpha$ RMSDs of AcrA-4M mutants along the MD trajectories, a figure of structure comparisons between the average structure of the largest cluster of Model 1-4M and the initial structure of wild type Model 1, and the figure of $C\alpha$ RMSF of Model 2 under pH 7.0 and pH 5.0. This material is available free of charge via the Internet at <http://pubs.acs.org>.

■ AUTHOR INFORMATION

Corresponding Author

*Fax:+86-21-65641740. E-mail: wnwang@fudan.edu.cn.

Notes

The authors declare no competing financial interest.

■ ACKNOWLEDGMENTS

This work was supported by National Major Basic Research Program of China (2009CB918600 and 2011CB808505), National Science Foundation of China (20973040 and 31070642), Science & Technology Commission of Shanghai Municipality (08DZ2270500), and Shanghai Leading Academic Discipline Project (B108). We are grateful to the computer center of Fudan University for their allocation of computer time.

■ REFERENCES

- (1) Zgurskaya, H. I.; Nikaido, H. *Mol. Microbiol.* **2000**, *37*, 219.
- (2) Murakami, S. *Curr. Opin. Struct. Biol.* **2008**, *18*, 459.
- (3) Murakami, S.; Nakashima, R.; Yamashita, E.; Matsumoto, T.; Yamaguchi, A. *Nature* **2006**, *443*, 173.
- (4) Murakami, S.; Nakashima, R.; Yamashita, E.; Yamaguchi, A. *Nature* **2002**, *419*, 587.
- (5) Sennhauser, G.; Amstutz, P.; Briand, C.; Storchenegger, O.; Grutter, M. G. *PLoS Biol.* **2007**, *5*, 106.
- (6) Seeger, M. A.; Schiefer, A.; Eicher, T.; Verrey, F.; Diederichs, K.; Pos, K. M. *Science* **2006**, *313*, 1295.
- (7) Yu, E. W.; McDermott, G.; Zgurskaya, H. I.; Nikaido, H.; Koshland, D. E. *Science* **2003**, *300*, 976.
- (8) Federici, L.; Walas, F.; Luisi, B. *Curr. Sci.* **2004**, *87*, 190.
- (9) Koronakis, V.; Eswaran, J.; Hughes, C. *Annu. Rev. Biochem.* **2004**, *73*, 467.
- (10) Koronakis, V.; Sharff, A.; Koronakis, E.; Luisi, B.; Hughes, C. *Nature* **2000**, *405*, 914.
- (11) Lobedanz, S.; Bokma, E.; Symmons, M. F.; Koronakis, E.; Hughes, C.; Koronakis, V. *Proc. Natl. Acad. Sci. U.S.A.* **2007**, *104*, 4612.
- (12) Gerken, H.; Misra, R. *Mol. Microbiol.* **2004**, *54*, 620.
- (13) Husain, F.; Humbard, M.; Misra, R. *J. Bacteriol.* **2004**, *186*, 8533.
- (14) Elkins, C. A.; Nikaido, H. *J. Bacteriol.* **2003**, *185*, 5349.
- (15) Ge, Q.; Yamada, Y.; Zgurskaya, H. *J. Bacteriol.* **2009**, *191*, 4365.
- (16) Zgurskaya, H. I.; Nikaido, H. *J. Mol. Biol.* **1999**, *285*, 409.
- (17) Mikolosko, J.; Bobyk, K.; Zgurskaya, H. I.; Ghosh, P. *Structure* **2006**, *14*, 577.
- (18) Symmons, M. F.; Bokma, E.; Koronakis, E.; Hughes, C.; Koronakis, V. *Proc. Natl. Acad. Sci. U.S.A.* **2009**, *106*, 7173.
- (19) Tikhonova, E. B.; Zgurskaya, H. I. *J. Biol. Chem.* **2004**, *279*, 32116.
- (20) Zgurskaya, H. I.; Nikaido, H. *J. Bacteriol.* **2000**, *182*, 4264.
- (21) Bagai, I.; Liu, W.; Rensing, C.; Blackburn, N. J.; McEvoy, M. M. *J. Biol. Chem.* **2007**, *282*, 35695.
- (22) Ferguson, K. M.; Lemmon, M. A.; Schlessinger, J.; Sigler, P. B. *Cell* **1995**, *83*, 1037.
- (23) Ingelman, M.; Bianchi, V.; Eklund, H. *J. Mol. Biol.* **1997**, *268*, 147.
- (24) Borges-Walmsley, M. I.; Beauchamp, J.; Kelly, S. M.; Jumel, K.; Candlish, D.; Harding, S. E.; Price, N. C.; Walmsley, A. R. *J. Biol. Chem.* **2003**, *278*, 12903.
- (25) Vaccaro, L.; Koronakis, V.; Sansom, M. S. P. *Biophys. J.* **2006**, *91*, 558.
- (26) Ip, H.; Stratton, K.; Zgurskaya, H.; Liu, J. *J. Biol. Chem.* **2003**, *278*, 50474.
- (27) Xu, Y.; Lee, M.; Moeller, A.; Song, S.; Yoon, B.-Y.; Kim, H.-M.; Jun, S.-Y.; Lee, K.; Ha, N.-C. *J. Biol. Chem.* **2011**, *286*, 17910.
- (28) Tikhonova, E. B.; Yamada, Y.; Zgurskaya, H. I. *Chem. Biol.* **2011**, *18*, 454.
- (29) Arnold, K.; Bordoli, L.; Kopp, J.; Schwede, T. *Bioinformatics* **2006**, *22*, 195.
- (30) Phillips, J. C.; Braun, R.; Wang, W.; Gumbart, J.; Tajkhorshid, E.; Villa, E.; Chipot, C.; Skeel, R. D.; Kale, L.; Schulten, K. *J. Comput. Chem.* **2005**, *26*, 1781.
- (31) MacKerell, A. D.; Feig, M.; Brooks, C. L. *J. Am. Chem. Soc.* **2004**, *126*, 698.
- (32) Jorgensen, W. L.; Chandrasekhar, J.; Madura, J. D.; Impey, R. W.; Klein, M. L. *J. Chem. Phys.* **1983**, *79*, 926.
- (33) Darden, T.; York, D.; Pedersen, L. *J. Chem. Phys.* **1993**, *98*, 10089.
- (34) Humphrey, W.; Dalke, A.; Schulter, K. *J. Mol. Graphics* **1996**, *14*, 33.
- (35) Gordon, J. C.; Myers, J. B.; Folta, T.; Shoja, V.; Heath, L. S.; Onufriev, A. *Nucleic Acids Res.* **2005**, *33*, W368.
- (36) Daura, X.; Gademann, K.; Jaun, B.; Seebach, D.; van Gunsteren, W. F.; Mark, A. E. *Angew. Chem., Int. Ed.* **1999**, *38*, 236.
- (37) Higgins, M. K.; Bokma, E.; Koronakis, E.; Hughes, C.; Koronakis, V. *Proc. Natl. Acad. Sci. U.S.A.* **2004**, *101*, 9994.
- (38) Wilks, J. C.; Slonczewski, J. L. *J. Bacteriol.* **2007**, *189*, 5601.